Long distance retrograde degeneration of the retino-geniculo-cortical pathway in homonymous hemianopia

Alekya P. Rajanala[1], Mohammad A. Shariati[1], and Yaping Joyce Liao[1,2]*

[1]Department of Ophthalmology, Stanford University School of Medicine, Stanford, CA, USA

[2]Department of Neurology, Stanford University School of Medicine, Stanford, CA, USA

* Corresponding author

Email: yjliao@stanford.edu (YJL)

Abstract

Long-distance retrograde degeneration of the retino-geniculo-cortical pathway has been described in humans and animal models following injury to the brain. In this study, we used optical coherence tomography (OCT) to measure the severity and timing of retrograde degeneration after post-chiasmal visual pathway lesions in patients with homonymous hemianopia. We performed a retrospective study of 69 patients with homonymous hemianopia and analyzed high quality OCT macular ganglion cell complex (GCC) and retinal nerve fiber layer (RNFL). Patients with lesions involving the optic tract and thalamus were included in the anterior group, while patients with lesions of the occipital lobe were included in the posterior group. Statistical significance was determined using Mann-Whitney U test and Wilcoxon test. We found that in patients with homonymous hemianopia, those with anterior lesion exhibited earlier and more severe thinning compared with the posterior group. In fact, thinning can occur within 2 months after insult in the anterior group. Within 6 months of onset, the anterior group exhibited about 5 times more hemi-macular GCC thinning than those with acquired lesions of the posterior visual pathway (P = 0.0023). Although the severity of hemi-macular GCC thinning was different, the majority of hemi-macular thinning occurred within the first 6 months in both groups. Beyond 2 years, thinning in those with acquired anterior and posterior lesions was minimal, except in a small number of patients with multiple insults to the occipital lobe. In conclusion, using OCT, we measured the severity and rate of long-distance, retrograde degeneration in patients with homonymous hemianopia. Homonymous hemi-macular thinning after optic tract and thalamic injury was more severe and occurred earlier compared with thinning after

36 occipital lobe insult via trans-synaptic degeneration. The presence of severe hemi-
37 macular degeneration on OCT provides objective evidence that localizes the lesion to
38 the post-chiasmal anterior visual pathway.
39

Introduction

The retino-geniculo-cortical visual pathway is a 3-neuron long-distance white matter pathway, and insult to any part of this pathway leads to devastating vision loss. Although vision loss in one eye can be compensated somewhat by using the remaining good eye to function, injury posterior to the optic chiasm is associated with homonymous hemianopia, which means one lesion in the brain leads to loss of the left or right side of vertical midline in both eyes. Homonymous visual field defect is most commonly due to stroke, and of these, most are due to occipital stroke [1-3]. Among 850 patients with 904 events causing homonymous hemianopia that were confirmed by neuroimaging, 70% were due to stroke (4% bilateral), and 30% were due to other conditions, such as trauma (14%), brain tumor (12%), neurosurgical procedures (2.5%), and multiple sclerosis (1.5%) [4]. Homonymous hemianopia cannot be easily compensated since both eyes are affected, and it leads to severe disability because patients can lose their driving eligibility. There is also disability due to hemianopic dyslexia [5, 6], deterioration of mental health [7, 8], and impairment of activities of daily living [9-11].

Retrograde long-distance degeneration occurs after visual field loss. This has been described after optic neuritis [12] and chiasmal compression [13], which involves degeneration of the optic nerve (up to about 5 centimeters) and loss of the retinal ganglion cell somata. After occipital lobe insult, degeneration across the retino-geniculo-cortical pathway can occur in a retrograde fashion trans-synaptically over 20 centimeters [14, 15]. The most definitive studies of retrograde trans-synaptic degeneration have been done with ablation of the striate cortex in non-human primates,

which have shown that within 14-100 days, retrograde degeneration extends from the occipital lobe into the lateral geniculate, optic tract, and the eye [16, 17]. Retrograde trans-synaptic degeneration of the visual pathway has also been described in human autopsy and MRI studies [18-21].

Advances in optical coherence tomography (OCT) means that we now have a reliable *in vivo* method of measuring long-distance, retrograde degeneration of the visual pathway in humans at point-of-care locations such as the eye clinic [22, 23]. Commercial spectral-domain OCT machines provide resolution of 3-5 microns, which allow for quantification of individual retinal layers comparable to that of retinal histology [24, 25]. Advances in OCT segmentation means we can routinely segment the thickness of the layer containing retinal ganglion cells (ganglion cell layer or GCC) and the thickness of the layer containing unmyelinated retinal ganglion cell axons (retinal nerve fiber layer or RNFL). Modern OCT machines also have eye tracking, which allows for good inter-scan reproducibility [26-28], which facilitates comparison of OCT measurements over time. OCT measurements have been useful in measuring changes in thickness in different retinal layers due to optic nerve diseases, such as glaucoma, optic neuritis, ischemic optic neuropathy, papilledema, and traumatic optic neuropathy [29-32].

In this study, we aimed to measure the severity and rate of retrograde degeneration after onset of homonymous hemianopia. We recruited patients with homonymous visual field defect and used OCT to measure the severity and timing of retrograde degeneration after injury to the post-chiasmal visual pathway. In particular, we compared measurements between lesions affecting the anterior post-chiasmal

pathway, involving the optic tract and the thalamus, with lesions of the posterior post-chiasmal pathway, involving the occipital lobe. Understanding how an insult to one region of the brain affects white matter tracts and neuronal survival elsewhere is important from a biological as well as therapeutic standpoint.

Methods

Patient Selection

Our study was approved by the Stanford Institutional Review Board. We performed a retrospective case review of 79 consecutive patients seen in 2012-2017 and identified 69 patients (51% male), 138 eyes, and 73 events with homonymous visual field defect. Thirty-one patients (45%) had left-sided lesions, and 34 patients (49%) had right-sided lesions. Four patients (6%) had with bilateral, sequential strokes. Thirty-six patients (52%) had 2 or more OCTs. Mean age of all patients was 54.7 ± 2.5 years (median 57 years, range 15-91 years). Mean age at onset of disease was 41 ± 4.7 years for the anterior group and 61.3 ± 2.5 years for the posterior group. Mean age for the congenital group was 41.4 ± 8.6 years. All patients were followed for at least one year, and 21 (30%) were followed for 2 years or more.

We included patients who had formal visual field testing to confirm presence of homonymous visual field defect in both eyes. This was done with automated static perimetry (Humphrey Visual Field Analyzer, Carl Zeiss Meditec, Germany) or manual perimetry (Goldmann Visual Field model, Haag-Streit, USA). Each patient had to have average mean deviation $\leq$ -3 dB on static perimetry or at least partial quadrantanopia on Goldmann visual field testing. Those with visual field loss affecting less than one

quadrant (e.g. homonymous scotomas) were excluded. We excluded patients with ophthalmic or neurological conditions of the visual pathway that could potentially affect the measurements.

Brain imaging was performed in all patients to confirm location and etiology of the visual field loss. Lesions involving the anterior post-chiasmal visual pathway, which involved the optic tract and the lateral geniculate nucleus, were considered to be in the anterior group. Lesions not involving the latter structures and primarily involving the occipital lobe were in the posterior group. One patient who had both anterior and posterior involvement due to multi-focal stroke was classified into the anterior group because of the involvement of the anterior structures. All patients with posterior cerebral artery strokes were included in the posterior group, regardless of stroke size. Four patients (6%) had bilateral posterior lesions and therefore did not have an “unaffected” side; these patients’ OCT and visual field data were analyzed without assigned control values.

We analyzed Humphrey Visual Field (HVF) data by mean deviation (dB) of the nasal and temporal hemifield using the Hood-Kardon linear model [22, 23]. The contralateral temporal field and ipsilateral nasal field were averaged as “abnormal” and the contralateral nasal field and ipsilateral temporal field were averaged as “control”. There was no difference in visual field severity between the anterior and the posterior group (anterior: -8.1 ± 2.2 dB, N = 7; posterior: -11.6 ± 1.6 dB, N = 33; P = 0.4011, Mann-Whitney).

Optical Coherence Tomography Data Acquisition

To assess changes in retinal thickness over time, we performed spectral-domain optical coherence tomography (OCT) (Cirrus HD-OCT model, Carl Zeiss Meditec, Dublin, CA, USA). Because age-related OCT thinning is relatively modest, at 1 μm of GCC or 2 μm of RNFL every decade [24, 25], the changes we measure over time likely reflected changes corresponding to the homonymous visual field defect. We performed the Macular Cube 512 x 128 and the Optic Disc 200 x 200 scans per manufacturer's instructions. We used high-resolution optical coherence tomography with eye-tracking capabilities and followed patients longitudinally as early as 1 week and up to 5 years after lesion onset. Only images with signal strength of 7 or above were included in the analysis. A total of 225 OCT (112 GCC; 113 RNFL) scans were performed. Nineteen scans were rejected based on poor segmentation, and 102 GCC and 104 RNFL scans were included in our analyses. All calculations were automatically segmented using the Zeiss algorithm and visually inspected to ensure appropriate segmentation.

Macular Ganglion Cell Complex OCT Analysis

On OCT, macular GCC thickness was measured as the combined thickness of the ganglion cell layer and the inner plexiform layer. We calculated the GCC thickness corresponding to the side of visual field loss (the "abnormal" side) and the side with normal visual field (the "control" side) by averaging the measurements in the two eyes [33, 34]. For example, in a patient with left homonymous visual field defect, the abnormal side was calculated as the average of the right eye superior temporal and inferior temporal hemi-macular GCC and the left eye superior nasal and inferior nasal GCC. The control side was the average of the right eye superior nasal and inferior nasal

GCC and the left eye superior temporal and inferior temporal GCC. To calculate the amount of GCC thinning for each subject, we subtracted the abnormal side from the control side [33]. To compare GCC thickness in the abnormal and control side in patients in the anterior and posterior groups, only 1 measurement per subject was used. If a patient had more than one OCT measurements, then the most recent OCT measurement was used. The range of abnormal GCC thickness was 43.5 to 74.5 μm in the anterior group, 45.8 to 91.3 μm in the acquired posterior group, and 43 to 77.5 μm in the congenital/incidental posterior group. Four patients in the anterior group, 4 patients in the posterior acquired group, and 1 patient in the posterior congenital group had very thin measurements that we visually confirmed was correctly measured.

To calculate the crossed GCC thickness measurements, we calculated the average thickness of the superior nasal and inferior nasal GCC. The non-crossed GCC thickness was calculated as the average thickness of the superior temporal and inferior temporal GCC. For example, in left homonymous visual field defect patients, the abnormal crossed GCC thickness was the average superior nasal and inferior nasal GCC in the left eye, and the control crossed GCC thickness was the average superior nasal and inferior nasal GCC in the right eye. In the same patient subgroup, the abnormal non-crossed GCC thickness was the average superior temporal and inferior temporal GCC in the right eye, and the control non-crossed GCC thickness was the average superior temporal and inferior temporal GCC in the left eye.

Retinal Nerve Fiber Layer OCT Analysis

RNFL thickness measurement was calculated as the average of the crossed and non-crossed fibers in both eyes [33]. Unlike the GCC, which demonstrates clear segregation of the crossed and the non-crossed visual pathways into the nasal and temporal retinae, respectively, all 4 quadrants of the RNFL contain a combination of crossed and non-crossed fibers. However, the nasal quadrant is known to contain preferentially more crossed fibers, while the superior, inferior, and temporal quadrants contain a majority of non-crossed fibers [23, 35]. Therefore, we analyzed crossed fibers using nasal quadrants, with nasal retina contralateral to the brain lesion as “abnormal” and ipsilateral nasal retina as “control.” We then analyzed non-crossed fibers as an average of superior and inferior quadrants of RNFL; superior and inferior retina ipsilateral to the brain lesion were defined as “abnormal” and contralateral superior and inferior retina as “control”. The temporal quadrant was not included in this particular analysis because it is relatively much thinner than the superior and the inferior quadrants. The non-crossed fibers were then separately analyzed again as an average of superior, inferior, and temporal quadrants of RNFL; ipsilateral superior, inferior, and temporal retina were defined as “abnormal” and contralateral superior, inferior, and temporal retina as “control” [33].

Statistical Analysis

We used the non-parametric Mann-Whitney U test and the non-parametric Wilcoxon matched-pairs signed rank test in Prism (GraphPad; La Jolla, CA), and used Prism to plot the data. The cut-off for significant values was set at $P < 0.05$. All data were presented as mean ± standard error of mean (SEM).

Results

Patient Characteristics

We performed a case-control study of 69 patients with homonymous hemianopia in order determine how optical coherence tomography (OCT) measurements change over time (Table 1). There were 15 patients with lesions involving the anterior post-chiasmal visual pathway, including the optic tract and thalamus (lateral geniculate nucleus). This group was called the “anterior” group because of involvement of the immediate post-chiasmal structures, even if the insult included nearby structures (e.g. temporal lobe). All lesions in the anterior group were acquired, and the most common causes included traumatic brain injury, tumors, and hemorrhage. There were 54 patients with lesions involving the posterior post-chiasmal visual pathway, including the occipital lobe and sometimes occipito-temporal or occipito-parietal lobes (tumors, arteriovenous malformation). This group was called the “posterior” group because the lesions involved structures beyond the lateral geniculate nucleus and did not involve the immediate post-chiasmal structures. Forty-seven patients in the posterior group had acquired lesions, most commonly due to posterior cerebral artery strokes and tumors. Seven patients in the posterior group had congenital or incidentally found occipital atrophy and were analyzed separately.

Table 1. Clinical Features of Patients with Homonymous Visual Field Defect

	Anterior	Posterior
	15	54

Number of Patients		
Age (yrs) (Mean ± SEM)	41 ± 4.7 (range: 15-77, median 40)	58.5 ± 2.7 (16 – 91, median 62)
Gender (Female : Male) (%)	7 : 8 (47 / 53)	27 : 27 (50 / 50)
Etiologies		
Stroke	2	40*
Tumor	3	8
Trauma	8	0
Hemorrhage	2	3
Incidental	0	7

*4 with bilateral strokes

An example patient in the anterior group is a 51-year-old man with acute onset vision loss due to hypertensive thalamic hemorrhage (Fig 1A, 1C, and 1E). His systolic blood pressures were over 200 mm Hg, and the hemorrhage involved the right optic tract in the thalamus and lateral geniculate nucleus as seen on brain magnetic resonance imaging (MRI) (Fig 1A). Kinetic perimetry with Goldmann visual field test revealed homonymous left inferior quadrantanopia (Fig 1C). OCT macular GCC analysis 2 months after onset revealed prominent thinning of the corresponding macula

in a homonymous, hemi-macular pattern, which involved the temporal macula in the right eye and nasal macula in the left eye (Fig 1E).

An example patient in the "posterior" group is a 38-year-old woman with systemic lupus erythematosus who developed a right posterior cerebral artery stroke in the setting of 5 days of fever, vomiting, and diarrhea after a dental procedure (Fig 1B, 1D, and 1F). Brain MRI revealed restricted diffusion and hyperintensity on T2-weighted images (Fig 1B). Her Goldmann visual field test showed a left homonymous hemianopia (Fig 1D). In contrast to the anterior patient, her OCT macular GCC performed 3 months after onset revealed no thinning in either eye (Fig 1F). Thus, there was a dramatic difference between the anterior patient, who exhibited severe macular GCC thinning, and the posterior patient, who exhibited normal macular GCC measurements within 2 months after insult.

Fig 1: Representative example of homonymous visual field defect after insult involving the anterior (A, C, E) or the posterior (B, D, F) post-chiasmal visual pathway. A. Brain magnetic resonance imaging (MRI) axial gradient recall echo (GRE) and axial FLAIR (fluid-attenuated inversion recovery) scans showing right thalamic hemorrhage associated with hypertension (yellow arrows). The hemorrhage and edema involved the right optic tract within the basal ganglia and the lateral geniculate nucleus. **B.** Brain MRI axial diffusion weighted imaging (DWI) and axial T_2-weighted scans showing stroke (yellow arrows) in the right posterior cerebral artery territory. **C**. Kinetic perimetry for anterior patient showing homonymous left inferior quadrantanopia. **D.** Kinetic perimetry for posterior patient showing homonymous left hemianopia. **E**. OCT

macular GCC analysis for the anterior patient 2 months after onset of vision loss exhibited homonymous hemi-macular thinning involving the right eye temporal and left eye nasal maculae. There was a GCC thickness difference of 21.5 μm between the abnormal side (average of right eye temporal GCC and left eye nasal GCC) and control side (average of right eye nasal GCC and left eye temporal GCC) (abnormal: 59.8 μm, control: 81.3 μm). **F.** OCT macular GCC analysis for the posterior patient 3 months after onset of vision loss exhibited no thinning in either eye.

Significantly greater GCC thinning in anterior group

To determine whether the difference in macular GCC was present in all patients in the anterior and the posterior groups, we included one mean macular GCC measurement per patient and compared GCC thickness corresponding to the side of visual field loss ("abnormal" side) and the side corresponding with normal visual field ("control" side) in patients with acquired lesions (see Methods). In the anterior group, the abnormal side had 23.1 μm thinner GCC relative to the control side (abnormal: 56.5 ± 2.6 μm, control: 79.6 ± 1.5 μm, N = 15, $P < 0.0001$, Wilcoxon signed-rank test) (Fig 2B), while the posterior group, had 6.6 μm thinner GCC in the abnormal side (abnormal: 69.9 ± 1.6 μm, control: 76.5 ± 1.2 μm, N = 41, $P < 0.0001$, Wilcoxon). This means that among patients with acquired lesions, the anterior group had 3.5 times greater GCC thinning between the abnormal and the control side compared with the posterior group ($P < 0.0001$, Mann-Whitney). There was no significant difference between the control sides of the anterior and posterior groups ($P = 0.223$, Mann-Whitney). To make sure the differences we observed between the anterior and posterior groups were not related to

variable time since onset, we normalized the GCC thickness by time (months since onset) and found that in anterior group, the rate of GCC thinning was much faster compared with the posterior group (anterior: 4.6 ± 1.1 μm/month, N = 13; posterior: 0.2 ± 0.5 μm/month, N = 36; P = 0.0002, Mann-Whitney) (Fig 2C). In 7 patients with congenital or incidentally noted occipital atrophy, there was 20.0 μm greater thinning in the abnormal side compared with the control side (abnormal: 58.1 ± 4.3 μm, control: 78.1 ± 3.0 μm, N = 7, P = 0.0156, Wilcoxon), which was not as severe as the anterior group but more severe than the acquired posterior group.

We asked whether there was a difference in retrograde degeneration of the crossed and the non-crossed pathways after acquired lesions of the visual pathway, since the crossed pathway is slightly longer [35, 36]. On macular GCC measurements, there was no significant difference in thinning when comparing the crossed vs. non-crossed pathway. There was 3.1 times as much crossed GCC thinning in the anterior group compared to the posterior group, and 3.5 times as much non-crossed GCC thinning in the anterior versus posterior group (Table 2) (Fig 2D-E).

Fig 2: Significantly greater GCC thinning corresponding to visual field loss in the anterior group compared with the posterior group. A. An example of OCT ganglion cell analysis. The averaged red wedges represent “abnormal” and the averaged blue wedges represent “control” GCC thickness in a patient with right homonymous visual field defect. **B-F.** Graphs showing GCC thickness and rate of GCC thinning (OU, crossed, and non-crossed) for patients with anterior versus posterior visual pathway lesions. All graphs show significant differences for GCC between anterior and posterior

299 groups. Error bars represent standard error of mean. *P between 0.01 to 0.05, **P

300 between 0.001 to 0.01, and ***P < 0.001.

301

302 **Table 2: Amount of Crossed and Non-Crossed GCC and RNFL Thinning.**

	Anterior				Posterior				P-value
	N	Abnormal (µm)	Control (µm)	Dif (µm)	N	Abnormal (µm)	Control (µm)	Dif (µm)	
Crossed GCC	15	55.1 ± 2.6	79.0 ± 1.8	23.9	41	69.0 ± 1.7	76.7 ± 1.3	7.7	**<0.0001**[a] **<0.0001**[b] **<0.0001**[c]
Non-Crossed GCC	15	57.9 ± 2.6	80.3 ± 1.4	22.4	41	70.0 ± 1.5	76.4 ± 1.1	6.4	**<0.0001**[a] **<0.0001**[b] **<0.0001**[c]
Crossed RNFL	14	57.7 ± 2.4	69.4 ± 2.9	11.6	42	65.7 ± 1.7	66.4 ± 1.9	1.5	**0.**0284[a] 0.2810[b] **0.0078**[c]
Non-Crossed RNFL (S/I)	14	87.5 ± 5.4	99.2 ± 4.0	11.7	42	105.2 ± 2.7	107.7 ± 2.5	1.6	**0.0017**[a] 0.3900[b] **0.0055**[c]
Non-Crossed RNFL (S/I/T)	14	74.7 ± 4.6	83.9 ± 3.4	9.2	42	90.6 ± 2.1	92.7 ± 2.0	2.1	**0.0012**[a] 0.4800[b] **0.0047**[c]

303 Dif: difference
304 [a] Wilcoxon between Anterior Abnormal and Anterior Control
305 [b] Wilcoxon between Posterior Abnormal and Posterior Control
306 [c] Mann-Whitney between Anterior Amount of Thinning and Posterior Amount of Thinning
307
308

309 **Table 3. Rate of Thinning (µm/month) of Crossed and Non-Crossed GCC and**

310 **RNFL.**

	Anterior	Posterior	P-value[a]
Crossed GCC	4.7 (N = 13)	0.7 (N = 35)	**0.0004**
Non-crossed GCC	4.5 (N = 13)	0.6 (N = 35)	**0.0002**
Crossed RNFL	2.3 (N = 12)	0.6 (N = 34)	0.1176

Non-Crossed RNFL (S/I)	1.5 (N = 12)	0.7 (N = 32)	0.076
Non-Crossed RNFL (S/I/T)	1.0 (N = 12)	0.7 (N = 32)	0.053

[a] Mann-Whitney between Anterior Rate of Thinning and Posterior Rate of Thinning

Majority of GCC thinning occurred within 6 months

Given the difference in rate of thinning of GCC between the anterior and the posterior groups, we looked at GCC data only within 2 years of onset. The anterior group exhibited GCC thinning by the first OCT measurement, which was as early as 2 months after lesion onset. Within 4 months, the anterior group showed significant 19.9 μm of GCC thinning (abnormal: 60.5 ± 2.0 μm, control: 80.5 ± 2.2 μm, N = 6, P = 0.0313, Wilcoxon signed-rank test) (Table 4) (Fig 3A). The posterior group showed significant 3.7 μm of GCC thinning at 24 months after lesion onset (abnormal: 72.6 ± 2.0 μm, control: 76.3 ± 1.6 μm, N = 23, P = 0.0416, Wilcoxon signed-rank test). However, by 6 months after lesion onset, the majority of GCC thinning had already occurred in both groups (anterior: 78%, posterior: 58%).

Fig 3: Timing and rate of macular GCC thinning in anterior and posterior groups. **A.** Cumulative difference between abnormal and normal GCC measurements in the anterior and posterior groups 2-24 months after onset. **B.** Bar graph showing rate of GCC thinning, calculated as cumulative difference between abnormal and normal GCC measurements normalized by time in months (mo). We binned the rate of thinning to show pattern of change at 0-3, 4-6, 7-12, and 13-24 months. All error bars represent standard error of mean.

Table 4. Time course of GCC thinning.

	Anterior				Posterior				P-value
	N	Abnormal (μm)	Control (μm)	Dif (μm)	N	Abnormal (μm)	Control (μm)	Dif (μm)	
< 2 mo	3	63.3 ± 3.3	77.8 ± 2.4	14.5	9	73.6 ± 2.6	75.2 ± 2.8	1.6	0.2500[a] 0.2344[b] **0.0182**[c]
<3 mo	5	61.5 ± 2.1	79.1 ± 2.0	17.6	11	71.7 ± 3.4	74.5 ± 2.4	2.7	0.0625[a] 0.3105[b] **0.0060**[c]
<4 mo	6	60.5 ± 2.0	80.5 ± 2.2	19.9	12	72.3 ± 3.2	74.5 ± 2.2	2.2	**0.0313**[a] 0.5625[b] **0.0014**[c]
< 6 mo	7	62.1 ± 2.3	80.3 ± 1.9	18.1	15	71.8 ± 2.9	75.6 ± 2.0	3.8	**0.0156**[a] 0.1879[b] **0.0023**[c]
< 12 mo	9	59.6 ± 2.4	81.7 ± 1.7	22.1	20	72.2 ± 2.2	75.9 ± 1.7	4.1	**0.0039**[a] 0.0531[b] **<0.0001**[c]
< 24 mo	10	59.4 ± 2.2	81.2 ± 1.6	21.8	23	72.6 ± 2.0	76.3 ± 1.6	3.7	**0.0020**[a] 0.0416[b] **<0.0001**[c]
All	15	56.5 ± 2.6	79.6 ± 1.5	23.1	47	69.9 ± 1.6	76.5 ± 1.2	6.6	**<0.0001**[a] **<0.0001**[b] **<0.0001**[c]

Dif: difference
[a] Wilcoxon between Anterior Abnormal and Anterior Control
[b] Wilcoxon between Posterior Abnormal and Posterior Control
[c] Mann-Whitney between Anterior Amount of Thinning and Posterior Amount of Thinning

Stable GCC thinning beyond 2 years except in patients with multiple insults

To determine whether more thinning occurred beyond 2 years, we examined 8 posterior lesion patients (total 10 events) who had 3 or more serial OCT measurements beyond 2 years (Fig 4B). Those with an isolated unilateral or bilateral occipital lobe event

demonstrated little to no (≤ 2 μm) further thinning beyond 2 years of lesion onset (all dashed lines in Fig 4B). In comparison, 2 patients with metastatic cancer who underwent radiation therapy and more than one surgical resection were noted to have the largest amount of progressive macular thinning (7 μm and 18 μm decrease; solid orange and black lines in Fig 4B). One patient with an atypical venous stroke affecting the posterior temporal lobe had progressive thinning of 6 μm within 2-3 years, but no thinning beyond 3-4 years of onset (solid lime green line in Fig 4B). One patient with bilateral recurrent strokes showed progressive GCC thinning over time; there was 4 μm thinning within the first 3 years of a right occipital stroke and 8 μm thinning around 2-4 years after a left-sided occipital stroke (solid red and light blue lines in Fig 4B). Her brain MRI showed multiple areas of involvement consistent with multiple stroke events, which may account for the progressive GCC thinning seen over time. In the anterior group, 2 patients had progressive GCC thinning (3 μm and 6 μm decrease; solid red and maroon lines in Fig 4A). Both of the latter patients had multiple lesions over time.

Fig 4: Serial GCC in anterior and posterior patients showed that many had stable GCC over years while some had further thinning. A. Macular GCC corresponding to the homonymous hemianopia in 6 anterior patients. Four had stable "abnormal" GCC thickness (dashed lines), while 2 had greater than 2 μm thinning (solid lines). **B.** Macular GCC corresponding to the visual field loss in 10 eyes in 8 patients in the posterior acquired group. Five events had stable GCC over years (dashed lines), while 5 events had progressive thinning beyond 2 years of lesion onset (solid lines; see details in Results).

RNFL thinning showed similar pattern of thinning as GCC

To determine whether there is a difference in thinning in the unmyelinated axonal layer compared with the retinal layer containing the retinal ganglion cells, we first performed an analysis of the crossed RNFL (nasal quadrants) pathway; significant thinning was seen in both the anterior and posterior groups (Table 2). The anterior group had significantly 7.7 times greater crossed RNFL thinning compared with the posterior group (Fig 5B). In the non-crossed RNFL (superior and inferior quadrants) pathway, there was significantly greater non-crossed RNFL thinning in the anterior group compared with the posterior group (Table 2) (Fig 5D-5E). The amount and rate of RNFL thinning was similar to what was seen in the GCC analysis in both the anterior and posterior groups. To confirm this, we correlate GCC and RNFL measurements using a Gaussian nonlinear fit. We analyzed the normal and abnormal thickness of the crossed pathway (nasal GCC vs. nasal quadrant of RNFL) and found strong correlation between GCC and RNFL measurements ($r^2 = 0.953$, N = 59, P = 0.985).

Fig 5: Greater RNFL thinning in anterior compared with the posterior group, and no difference in thinning between crossed and non-crossed pathways. A. Illustration of OCT retinal nerve fiber layer analysis. Blue wedge is the “control” and red wedge, the “abnormal” crossed RNFL quadrant in a patient with left homonymous visual field defect. **B.** Box-whisker plot of abnormal and control nasal crossed RNFL. **C.** Measurements in *B* normalized by time since onset in months (mo). **D.** Box-whisker plot of abnormal and control non-crossed RNFL, calculated as average of superior and

inferior quadrants (S/I). **E.** Box-whisker plot of abnormal and control non-crossed RNFL, calculated as average of superior, inferior, and temporal quadrants (S/I/T). **F.** Measurements in *D* and *E* normalized by time since onset in months (mo). Error bars represent standard error of mean. *P value between 0.01 to 0.05, **P value between 0.001 to 0.01, and ***P value less than 0.01.

Discussion

We performed a longitudinal study of anterior and posterior post-chiasmal lesions in patients with homonymous hemianopia to compare the severity and timing of retrograde degeneration of the retino-geniculo-cortical pathway. We found that anterior post-chiasmal visual pathway lesions led to prominent homonymous hemi-macular thinning within 2 months. One patient even had 9 μm thinning within one month. Within 3 months, the anterior group had 18 μm thinning or average rate of 8 μm per month. Within 6 months of onset, the anterior group exhibited about 5 times more GCC thinning than those with acquired lesions of the posterior visual pathway. *In contrast*, the posterior group had only 1.6 μm thinning at 2 months and 2.7 μm thinning at 3 months. At 3 months, posterior group had average rate of 1.4 μm per month, which was 33% that of the anterior group. After 6 months, there was relatively less thinning in both groups. Beyond 2 years, there was less than 2 μm thinning in both groups, except in a small number of patients who had multiple insults. Patients with congenital or incidentally noted posterior lesions had greater GCC thinning than those with acquired posterior lesions but less than patients with acquired anterior lesions. Both GCC and RNFL thinning were much more prominent and occurred earlier in the anterior group.

Although our study showed that both GCC and RNFL demonstrated similar patterns of degeneration, we found GCC analysis was better suited to study patients with homonymous hemianopia compared to RNFL analysis because of the clear segregation of neurons representing the nasal versus temporal visual fields. GCC analysis centers over the fovea and divides the crossed and non-crossed fibers into the nasal and temporal quadrants, making it simpler to classify abnormal and normal measurements. In our study, all GCC analysis (averaged, crossed, and non-crossed) was associated with more severe thinning and corresponded more strongly to homonymous visual field defect compared to all RNFL analysis (crossed, non-crossed). We observed that the averaged GCC, crossed GCC, and non-crossed GCC were similarly effective in examining retrograde degeneration. This is consistent with prior reports in the literature of patients with visual pathway lesions [33, 34, 37]. Comparison of timing of thinning of RNFL and GCC has also been studied in optic neuropathy patients, and GCC thinning has been reported earlier than RNFL thinning in disease processes like retrobulbar optic neuritis, papilledema, and anterior ischemic optic neuropathy [38, 39]. However, the GCC analysis is common to the Cirrus SD-OCT machine, which may not be consistently available in all eye clinics.

Following a lesion affecting the anterior post-chiasmal visual pathway, we found that retrograde non-trans-synaptic degeneration occurred significantly within 4 months and even as early as 2 months. Our findings are similar to what was found in previous small-scale human studies of anterior visual pathway lesions. Kanamori et al. studied 4 patients with optic tract lesion and noted mean 5.75 μm GCC thinning between 1 and 4 months after lesion onset, when comparing abnormal to control hemi-retinas [40]. A

longitudinal study by Gabilondo et al. reported 27.5 μm of GCC thinning between abnormal and control hemi-retinas 5 months after optic tract lesion in a multiple sclerosis patient [41]. In our study, we showed that after damage to the post-chiasmal anterior visual pathway, which included the optic tract, mean 14.5 μm of GCC thinning occurred within 2 months. Because there is only one neuronal synapse in between the lateral geniculate nucleus and retinal ganglion cells, lesions of the anterior visual pathway directly affect the retinal ganglion cell axons. Meanwhile, between the striate cortex and RGCs lies the lateral geniculate-striate synapse, so lesions of the posterior visual pathway likely receive neurotrophic support from neuronal connections at both ends. This theory of neurotrophic support is currently our best explanation for why lesions of the post-chiasmal anterior visual pathway are associated with more severe and rapid retinal thinning compared to lesions of the posterior visual pathway. We propose that the presence of severe hemi-macular degeneration on OCT may be useful to clinicians in localizing lesions to the post-chiasmal anterior visual pathway.

Evidence of retrograde trans-synaptic degeneration after posterior visual pathway damage has been historically controversial because of difficulties in performing large pathologic studies in humans. In contrast, there is clear evidence in a small number of animal studies that retinal thinning after occipital lesion can occur substantially as early as 1 year. A study of 2 adult New World marmoset monkeys by Hendrickson et al. reported 20% ganglion cell loss based on photomicrograph analysis of retinal section at 1 year after visual cortex lesion [15]. Cowey et al. studied 17 macaque monkeys and found that the RGC count ratio between abnormal to control hemiretina (based on histologic section of the eye contralateral to brain lesion) was 0.7

459 at 1 year, 0.4 at 2.5 years, and 0.4 at 8 years after unilateral striate cortex ablation [42].
460 Interestingly, though our study was performed *in vivo* in humans, the timing of retinal
461 thinning after visual cortex lesion is quite similar between our study and the non-human
462 primate studies [15, 42]. Furthermore, we reported that on longitudinal follow-up,
463 patients with occipital lobe damage did not demonstrate further retinal thinning after 2
464 years, which is consistent with the report by Cowey et al. of little to no RGC loss after
465 2.5 years after striate cortex ablation [42].

466 Human *in vivo* studies that used RNFL monitor retrograde trans-synaptic
467 degeneration after occipital insults had variability in the severity of thinning, likely
468 because of differences in methodology. We reported 3.1 μm of crossed RNFL thinning
469 within 2 years, which we calculated by comparing abnormal and control hemiretinas
470 between each individual patient (contralateral nasal retina for abnormal, ipsilateral nasal
471 retina for control). Jindahra et al. studied 26 posterior lesion patients and reported
472 average RNFL measurements of each eye; they observed 21.2 μm RNFL thinning in the
473 crossed eye and 18 μm in the non-crossed eye, when compared to eyes from control
474 patients [43]. Park et al. studied 46 patients with cerebral infarction affecting either
475 the posterior cerebral artery, middle cerebral artery, or anterior cerebral artery,
476 and reported 17.3 μm of crossed RNFL thinning [44] (when calculated using our paper's
477 methodology). Park et al. noted that time after stroke onset was significantly associated
478 with reduced mean RNFL thickness, but did not further describe timing of when
479 retrograde trans-synaptic degeneration first occurred. The majority of patients in the
480 Park study (30 patients, 65%) had RNFL measurements taken after 2 years and up to
481 20 years from lesion onset. Perhaps the greater severity of crossed RNFL thinning

reported by Park et al. is because of RNFL being measured much longer after lesion onset when compared to our study. It could also be due to their inclusion of patients with lesion of not only posterior cerebral artery territory but also middle and anterior cerebral artery territories. Gunes et al. studied 45 patients after MCA or PCA stroke and found little to no crossed RNFL thinning (-1.9 μm) [45], and Herro et al. noted 0 μm of crossed RNFL thinning in 9 occipital stroke patients [33]. The RNFL measurements from the latter two studies [33, 45] were calculated by the same methodology as our study and are more consistent with the changes our study found.

Human studies of patients with occipital lobe lesion have reported GCC measurements comparable to our finding of 4.1 μm of GCC thinning at 1 year of lesion onset. Anjos et al. studied 12 posterior cerebral artery stroke patients and found 15.5 μm of GCC thinning at 4.3 years after lesion onset when comparing abnormal to control hemiretinas of each patient (methodology identical to our study) [46]. A study by Herro et al. of 9 patients between 3-14 months after occipital stroke reported 5.3 μm of GCC thinning between affected and unaffected hemi-retinas [33]. In general, as we discussed earlier, the decreased severity of RNFL thinning in comparison to severity of GCC thinning provides further evidence that GCC is superior to RNFL for studying retrograde degeneration of the visual pathway [33, 37].

A review by Dinkin et al. suggests that understanding the time course of retrograde trans-synaptic degeneration could help clinicians determine the time of onset of brain lesions found incidentally on imaging and prognosticate visual field loss over time in patients with visual pathway damage [47]. Our study followed patients longitudinally by tracking OCT measurements over time with some patients being

505 followed for more than 5 years, much longer than previously published studies on
506 retrograde degeneration of the visual pathway [48]. We found 7.2 μm/year of nasal
507 quadrant crossed RNFL thinning in posterior patients, which was comparable to
508 Jindahra's report of 4.4 μm/year of average RNFL thinning of the crossed *eye* [48]. We
509 found there was a steady worsening of GCC thinning from 2, 4, 6, to 12 months (1.6
510 μm, 2.2 μm, 3.8 μm, and 4.1 μm of thinning, respectively) after onset of posterior visual
511 pathway lesion. After 2 years, however, most of these patients did not exhibit further
512 increase in severity of GCC thinning over time. The patients that did continue to
513 demonstrate increasingly severe thinning beyond 2 years were the ones with multiple
514 insults to the visual pathway. This progressive trend of GCC thinning is especially
515 concerning and clinically important in patients with metastatic cancer, multiple
516 neurologic surgeries, radiation treatments, recurrent stroke, and other insults. The
517 progressive nature of retrograde degeneration in these patients with multiple insults are
518 occurring at a measurable scale and may be occurring at a smaller scale in other
519 patient groups with multiple insults, such as in patients with multiple concussions or
520 multiple sclerosis.

521 A limitation of this study is that it was conducted retrospectively, and longitudinal
522 measurements were limited by the number of OCT scans each patient already had in
523 their medical records. However, this meant we could include a relatively large number of
524 patients compared with previous publications, which provides a more comprehensive
525 view of patients with homonymous hemianopia. The study was also limited because
526 patients had diverse clinical presentations and severity of visual field loss. However, this
527 broader approach was also done in historically important, large studies of homonymous

hemianopia [1-4]. Just as the study by Zhang et al. [4] was superior because they used brain MRI to confirm lesion and provide anatomic correlation, our study provides an additional dimension of measurement by adding OCT and long-term follow-up to further understand this common and debilitating cause of vision loss.

Conclusions

Our study fills an important gap in our understanding of long-distance retrograde degeneration by comparing the severity, timing, and rate of GCC and RNFL thinning in a large number of patients with homonymous visual field defect. A relatively large human study of retrograde degeneration is only possible due to advances in OCT imaging and its ability to provide high-resolution, reproducible, quantitation of the visual pathway at point-of-care locations. We found that anterior post-chiasmal lesions led to severe thinning of the retino-geniculate pathway within 2 months, with about 5 times greater thinning and 3 times faster rate of thinning at 3 months. We confirmed that trans-synaptic degeneration does occur after insult to the occipital lobe. Our study may be relevant to what also occurs following insults to other long white matter pathways. Finally, our study provides a global understanding of long-distance white matter tract degeneration, which is particularly important in consideration of the timing and type of therapies targeting regeneration or functional recovery in patients with homonymous hemianopia [49, 50].

Acknowledgments

The authors have no acknowledgments.

References

1. Smith JL. Homonymous hemianopia. A review of one hundred cases. American journal of ophthalmology. 1962;54:616-23. Epub 1962/10/01. PubMed PMID: 13989472.
2. Trobe JD, Lorber ML, Schlezinger NS. Isolated homonymous hemianopia. A review of 104 cases. Archives of ophthalmology (Chicago, Ill : 1960). 1973;89(5):377-81. Epub 1973/05/01. doi: 10.1001/archopht.1973.01000040379005. PubMed PMID: 4697213.
3. Fujino TK, K.; Yamada, R. Homonymous hemianopia: a retrospective study of 140 cases. Neuro-ophthalmology (Aeolus Press). 1986;6:17-21.
4. Zhang X, Kedar S, Lynn MJ, Newman NJ, Biousse V. Homonymous hemianopias: clinical-anatomic correlations in 904 cases. Neurology. 2006;66(6):906-10. Epub 2006/03/29. doi: 10.1212/01.wnl.0000203913.12088.93. PubMed PMID: 16567710.
5. Trauzettel-Klosinski S, Brendler K. Eye movements in reading with hemianopic field defects: the significance of clinical parameters. Graefe's archive for clinical and experimental ophthalmology = Albrecht von Graefes Archiv fur klinische und experimentelle Ophthalmologie. 1998;236(2):91-102. Epub 1998/03/14. PubMed PMID: 9498119.
6. Schuett S. The rehabilitation of hemianopic dyslexia. Nature reviews Neurology. 2009;5(8):427-37. Epub 2009/07/08. doi: 10.1038/nrneurol.2009.97. PubMed PMID: 19581901.
7. Gall C, Mueller I, Franke GH, Sabel BA. Psychological distress is associated with vision-related but not with generic quality of life in patients with visual field defects after cerebral lesions. Mental illness. 2012;4(2):e12. Epub 2012/07/26. doi: 10.4081/mi.2012.e12. PubMed PMID: 25478113; PubMed Central PMCID: PMCPMC4253382.
8. Papageorgiou E, Hardiess G, Schaeffel F, Wiethoelter H, Karnath HO, Mallot H, et al. Assessment of vision-related quality of life in patients with homonymous visual field defects. Graefe's archive for clinical and experimental ophthalmology = Albrecht von Graefes Archiv fur klinische und experimentelle Ophthalmologie. 2007;245(12):1749-58. Epub 2007/07/27. doi: 10.1007/s00417-007-0644-z. PubMed PMID: 17653566.
9. Sand KM, Wilhelmsen G, Naess H, Midelfart A, Thomassen L, Hoff JM. Vision problems in ischaemic stroke patients: effects on life quality and disability. European journal of neurology. 2016;23 Suppl 1:1-7. Epub 2015/11/14. doi: 10.1111/ene.12848. PubMed PMID: 26563092.
10. de Haan GA, Heutink J, Melis-Dankers BJ, Brouwer WH, Tucha O. Difficulties in Daily Life Reported by Patients With Homonymous Visual Field Defects. Journal of neuro-ophthalmology : the official journal of the North American Neuro-Ophthalmology Society. 2015;35(3):259-64. Epub 2015/03/31. doi: 10.1097/wno.0000000000000244. PubMed PMID: 25815856.
11. Lane AR, Smith DT, Schenk T. Clinical treatment options for patients with homonymous visual field defects. Clinical ophthalmology (Auckland, NZ). 2008;2(1):93-

592 102. Epub 2008/03/01. PubMed PMID: 19668392; PubMed Central PMCID:
593 PMCPMC2698722.
594 12. Manogaran P, Samardzija M, Schad AN, Wicki CA, Walker-Egger C, Rudin M, et al.
595 Retinal pathology in experimental optic neuritis is characterized by retrograde
596 degeneration and gliosis. Acta neuropathologica communications. 2019;7(1):116. Epub
597 2019/07/19. doi: 10.1186/s40478-019-0768-5. PubMed PMID: 31315675; PubMed
598 Central PMCID: PMCPMC6637505.
599 13. Moon CH, Hwang SC, Ohn YH, Park TK. The time course of visual field recovery and
600 changes of retinal ganglion cells after optic chiasmal decompression. Investigative
601 ophthalmology & visual science. 2011;52(11):7966-73. Epub 2011/09/29. doi:
602 10.1167/iovs.11-7450. PubMed PMID: 21896856.
603 14. Johnson H, Cowey A. Transneuronal retrograde degeneration of retinal ganglion
604 cells following restricted lesions of striate cortex in the monkey. Experimental brain
605 research. 2000;132(2):269-75. Epub 2000/06/15. PubMed PMID: 10853951.
606 15. Hendrickson A, Warner CE, Possin D, Huang J, Kwan WC, Bourne JA. Retrograde
607 transneuronal degeneration in the retina and lateral geniculate nucleus of the V1-lesioned
608 marmoset monkey. Brain structure & function. 2015;220(1):351-60. Epub 2013/11/01.
609 doi: 10.1007/s00429-013-0659-7. PubMed PMID: 24173617.
610 16. Horoupian DS, Ghetti B, Wisniewski HM. Retrograde transneuronal degeneration of
611 optic fibers and their terminals in lateral geniculate nucleus of rhesus monkey. Brain
612 research. 1973;49(2):257-75. Epub 1973/01/30. PubMed PMID: 4198369.
613 17. Cowey A, Alexander I, Stoerig P. Transneuronal retrograde degeneration of retinal
614 ganglion cells and optic tract in hemianopic monkeys and humans. Brain : a journal of
615 neurology. 2011;134(Pt 7):2149-57. doi: 10.1093/brain/awr125. PubMed PMID:
616 21705429.
617 18. Beatty RM, Sadun AA, Smith L, Vonsattel JP, Richardson EP, Jr. Direct demonstration
618 of transsynaptic degeneration in the human visual system: a comparison of retrograde and
619 anterograde changes. Journal of neurology, neurosurgery, and psychiatry. 1982;45(2):143-
620 6. Epub 1982/02/01. PubMed PMID: 7069426; PubMed Central PMCID: PMCPMC1083042.
621 19. Bridge H, Jindahra P, Barbur J, Plant GT. Imaging reveals optic tract degeneration in
622 hemianopia. Investigative ophthalmology & visual science. 2011;52(1):382-8. doi:
623 10.1167/iovs.10-5708. PubMed PMID: 20739474.
624 20. Patel KR, Ramsey LE, Metcalf NV, Shulman GL, Corbetta M. Early diffusion evidence
625 of retrograde transsynaptic degeneration in the human visual system. Neurology.
626 2016;87(2):198-205. Epub 2016/06/17. doi: 10.1212/wnl.0000000000002841. PubMed
627 PMID: 27306632; PubMed Central PMCID: PMCPMC4940065.
628 21. Millington RS, Yasuda CL, Jindahra P, Jenkinson M, Barbur JL, Kennard C, et al.
629 Quantifying the pattern of optic tract degeneration in human hemianopia. Journal of
630 neurology, neurosurgery, and psychiatry. 2014;85(4):379-86. Epub 2013/10/29. doi:
631 10.1136/jnnp-2013-306577. PubMed PMID: 24163431.
632 22. Galetta KM, Calabresi PA, Frohman EM, Balcer LJ. Optical coherence tomography
633 (OCT): imaging the visual pathway as a model for neurodegeneration. Neurotherapeutics :
634 the journal of the American Society for Experimental NeuroTherapeutics. 2011;8(1):117-
635 32. doi: 10.1007/s13311-010-0005-1. PubMed PMID: 21274691; PubMed Central PMCID:
636 PMC3075740.

637 23. Chan NCY, Chan CKM. The use of optical coherence tomography in neuro-
638 ophthalmology. Current opinion in ophthalmology. 2017;28(6):552-7. Epub 2017/08/15.
639 doi: 10.1097/icu.0000000000000418. PubMed PMID: 28806189.
640 24. Cheng J, Sohn EH, Jiao C, Adler KL, Kaalberg EE, Russell SR, et al. Correlation of
641 Optical Coherence Tomography and Retinal Histology in Normal and Pro23His Retinal
642 Degeneration Pig. Translational vision science & technology. 2018;7(6):18. Epub
643 2018/12/07. doi: 10.1167/tvst.7.6.18. PubMed PMID: 30519502; PubMed Central PMCID:
644 PMCPMC6269133.
645 25. Xie W, Zhao M, Tsai SH, Burkes WL, Potts LB, Xu W, et al. Correlation of spectral
646 domain optical coherence tomography with histology and electron microscopy in the
647 porcine retina. Experimental eye research. 2018;177:181-90. Epub 2018/08/19. doi:
648 10.1016/j.exer.2018.08.003. PubMed PMID: 30120928; PubMed Central PMCID:
649 PMCPMC6348113.
650 26. Kim JS, Ishikawa H, Sung KR, Xu J, Wollstein G, Bilonick RA, et al. Retinal nerve fibre
651 layer thickness measurement reproducibility improved with spectral domain optical
652 coherence tomography. The British journal of ophthalmology. 2009;93(8):1057-63. Epub
653 2009/05/12. doi: 10.1136/bjo.2009.157875. PubMed PMID: 19429591; PubMed Central
654 PMCID: PMCPMC2861342.
655 27. Chin EK, Sedeek RW, Li Y, Beckett L, Redenbo E, Chandra K, et al. Reproducibility of
656 macular thickness measurement among five OCT instruments: effects of image resolution,
657 image registration, and eye tracking. Ophthalmic surgery, lasers & imaging : the official
658 journal of the International Society for Imaging in the Eye. 2012;43(2):97-108. Epub
659 2011/12/29. doi: 10.3928/15428877-20111222-02. PubMed PMID: 22201525.
660 28. Rebolleda G, Diez-Alvarez L, Casado A, Sanchez-Sanchez C, de Dompablo E,
661 Gonzalez-Lopez JJ, et al. OCT: New perspectives in neuro-ophthalmology. Saudi journal of
662 ophthalmology : official journal of the Saudi Ophthalmological Society. 2015;29(1):9-25.
663 Epub 2015/04/11. doi: 10.1016/j.sjopt.2014.09.016. PubMed PMID: 25859135; PubMed
664 Central PMCID: PMCPMC4314576.
665 29. Chen JJ. Optical Coherence Tomography and Neuro-Ophthalmology. Journal of
666 neuro-ophthalmology : the official journal of the North American Neuro-Ophthalmology
667 Society. 2018;38(1):e5-e8. Epub 2017/03/08. doi: 10.1097/wno.0000000000000505.
668 PubMed PMID: 28266953.
669 30. Kardon RH. Role of the macular optical coherence tomography scan in neuro-
670 ophthalmology. Journal of neuro-ophthalmology : the official journal of the North American
671 Neuro-Ophthalmology Society. 2011;31(4):353-61. Epub 2011/11/18. doi:
672 10.1097/WNO.0b013e318238b9cb. PubMed PMID: 22089499; PubMed Central PMCID:
673 PMCPMC3226727.
674 31. Sakamoto A, Hangai M, Nukada M, Nakanishi H, Mori S, Kotera Y, et al. Three-
675 dimensional imaging of the macular retinal nerve fiber layer in glaucoma with spectral-
676 domain optical coherence tomography. Investigative ophthalmology & visual science.
677 2010;51(10):5062-70. doi: 10.1167/iovs.09-4954. PubMed PMID: 20463326.
678 32. Sharma R, Sharma A, Arora T, Sharma S, Sobti A, Jha B, et al. Application of anterior
679 segment optical coherence tomography in glaucoma. Survey of ophthalmology.
680 2014;59(3):311-27. Epub 2013/10/22. doi: 10.1016/j.survophthal.2013.06.005. PubMed
681 PMID: 24138894.

682 33. Herro AM, Lam BL. Retrograde degeneration of retinal ganglion cells in
683 homonymous hemianopsia. Clinical ophthalmology (Auckland, NZ). 2015;9:1057-64. Epub
684 2015/06/20. doi: 10.2147/opth.s81749. PubMed PMID: 26089638; PubMed Central
685 PMCID: PMCPMC4468984.
686 34. Mitchell JR, Oliveira C, Tsiouris AJ, Dinkin MJ. Corresponding Ganglion Cell Atrophy
687 in Patients With Postgeniculate Homonymous Visual Field Loss. Journal of neuro-
688 ophthalmology : the official journal of the North American Neuro-Ophthalmology Society.
689 2015. Epub 2015/06/03. doi: 10.1097/wno.0000000000000268. PubMed PMID:
690 26035806.
691 35. De Moraes CG. Anatomy of the visual pathways. Journal of glaucoma. 2013;22 Suppl
692 5:S2-7. doi: 10.1097/IJG.0b013e3182934978. PubMed PMID: 23733119.
693 36. Kidd D. The optic chiasm. Clinical anatomy (New York, NY). 2014;27(8):1149-58.
694 Epub 2014/05/16. doi: 10.1002/ca.22385. PubMed PMID: 24824063.
695 37. Shin HY, Park HY, Choi JA, Park CK. Macular ganglion cell-inner plexiform layer
696 thinning in patients with visual field defect that respects the vertical meridian. Graefe's
697 archive for clinical and experimental ophthalmology = Albrecht von Graefes Archiv fur
698 klinische und experimentelle Ophthalmologie. 2014. doi: 10.1007/s00417-014-2706-3.
699 PubMed PMID: 25104464.
700 38. Kupersmith MJ, Garvin MK, Wang JK, Durbin M, Kardon R. Retinal Ganglion Cell
701 Layer Thinning Within One Month of Presentation for Non-Arteritic Anterior Ischemic
702 Optic Neuropathy. Investigative ophthalmology & visual science. 2016;57(8):3588-93.
703 Epub 2016/07/09. doi: 10.1167/iovs.15-18736. PubMed PMID: 27388052; PubMed
704 Central PMCID: PMCPMC5996873.
705 39. Kardon R. Optical coherence tomography in papilledema: what am I missing?
706 Journal of neuro-ophthalmology : the official journal of the North American Neuro-
707 Ophthalmology Society. 2014;34 Suppl:S10-7. Epub 2014/08/19. doi:
708 10.1097/wno.0000000000000162. PubMed PMID: 25133965.
709 40. Kanamori A, Nakamura M, Yamada Y, Negi A. Spectral-domain optical coherence
710 tomography detects optic atrophy due to optic tract syndrome. Graefe's archive for clinical
711 and experimental ophthalmology = Albrecht von Graefes Archiv fur klinische und
712 experimentelle Ophthalmologie. 2013;251(2):591-5. Epub 2012/07/05. doi:
713 10.1007/s00417-012-2096-3. PubMed PMID: 22760961.
714 41. Gabilondo I, Sepulveda M, Ortiz-Perez S, Fraga-Pumar E, Martinez-Lapiscina EH,
715 Llufriu S, et al. Retrograde retinal damage after acute optic tract lesion in MS. Journal of
716 neurology, neurosurgery, and psychiatry. 2013;84(7):824-6. Epub 2013/05/30. doi:
717 10.1136/jnnp-2012-304854. PubMed PMID: 23715916.
718 42. Cowey A, Stoerig P, Williams C. Variance in transneuronal retrograde ganglion cell
719 degeneration in monkeys after removal of striate cortex: effects of size of the cortical
720 lesion. Vision research. 1999;39(21):3642-52. Epub 2000/04/04. doi: 10.1016/s0042-
721 6989(99)00097-8. PubMed PMID: 10746134.
722 43. Jindahra P, Petrie A, Plant GT. Retrograde trans-synaptic retinal ganglion cell loss
723 identified by optical coherence tomography. Brain : a journal of neurology. 2009;132(Pt
724 3):628-34. doi: 10.1093/brain/awp001. PubMed PMID: 19224900.
725 44. Park HY, Park YG, Cho AH, Park CK. Transneuronal retrograde degeneration of the
726 retinal ganglion cells in patients with cerebral infarction. Ophthalmology.
727 2013;120(6):1292-9. doi: 10.1016/j.ophtha.2012.11.021. PubMed PMID: 23395544.

728 45. Gunes A, Inal EE, Demirci S, Tok L, Tok O, Demirci S. Changes in retinal nerve fiber
729 layer thickness in patients with cerebral infarction: evidence of transneuronal retrograde
730 degeneration. Acta neurologica Belgica. 2016;116(4):461-6. Epub 2016/01/07. doi:
731 10.1007/s13760-015-0592-z. PubMed PMID: 26732619.
732 46. Anjos R, Vieira L, Costa L, Vicente A, Santos A, Alves N, et al. Macular Ganglion Cell
733 Layer and Peripapillary Retinal Nerve Fibre Layer Thickness in Patients with Unilateral
734 Posterior Cerebral Artery Ischaemic Lesion: An Optical Coherence Tomography Study.
735 Neuro-ophthalmology (Aeolus Press). 2016;40(1):8-15. Epub 2016/12/09. doi:
736 10.3109/01658107.2015.1122814. PubMed PMID: 27928376; PubMed Central PMCID:
737 PMCPMC5123159.
738 47. Dinkin M. Trans-synaptic Retrograde Degeneration in the Human Visual System:
739 Slow, Silent, and Real. Current neurology and neuroscience reports. 2017;17(2):16. Epub
740 2017/02/24. doi: 10.1007/s11910-017-0725-2. PubMed PMID: 28229400.
741 48. Jindahra P, Petrie A, Plant GT. The time course of retrograde trans-synaptic
742 degeneration following occipital lobe damage in humans. Brain : a journal of neurology.
743 2012;135(Pt 2):534-41. doi: 10.1093/brain/awr324. PubMed PMID: 22300877.
744 49. Ajina S, Kennard C. Rehabilitation of damage to the visual brain. Revue
745 neurologique. 2012;168(10):754-61. Epub 2012/09/18. doi:
746 10.1016/j.neurol.2012.07.015. PubMed PMID: 22981268; PubMed Central PMCID:
747 PMCPMC3990209.
748 50. Schofield TM, Leff AP. Rehabilitation of hemianopia. Current opinion in neurology.
749 2009;22(1):36-40. Epub 2009/01/22. doi: 10.1097/WCO.0b013e32831f1b2c. PubMed
750 PMID: 19155760.
751

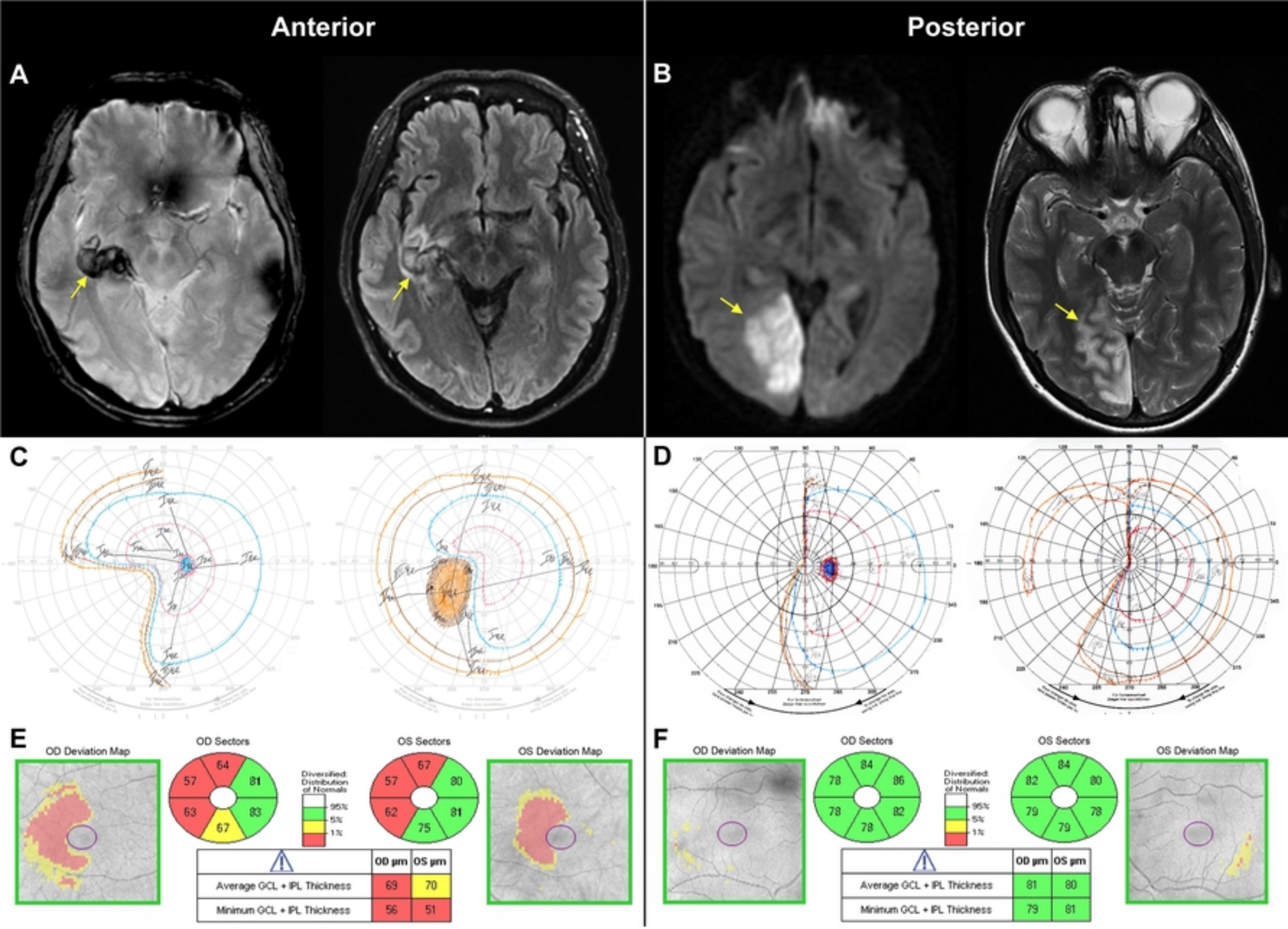
Anterior
Posterior
A
B
C
D
E
F
OD Deviation Map
OD Sectors
OS Sectors
OS Deviation Map
Diversified Distribution of Normals
95%
5%
1%
OD µm
OS µm
Average GCL + IPL Thickness
Minimum GCL + IPL Thickness
64
57
81
63
83
67
67
57
80
62
81
75
84
78
86
78
82
78
84
82
80
79
78
79
69
70
56
51
81
80
79
81

Figure 1

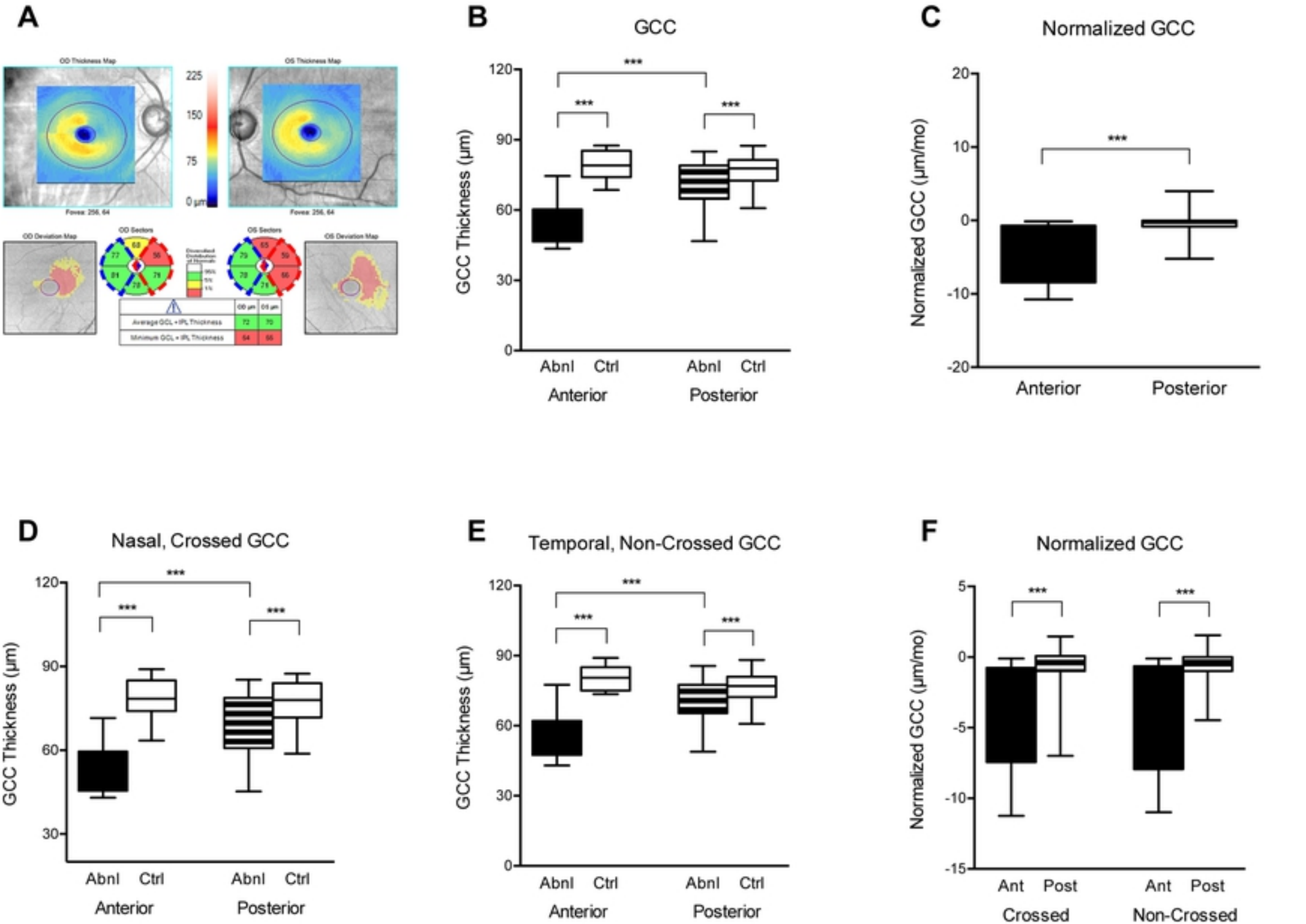
A
OD Thickness Map
OS Thickness Map
225
150
75
0 µm
Fovea: 256, 64
Fovea: 256, 64
OD Deviation Map
OD Sectors
OS Sectors
OS Deviation Map
Average GCL + IPL Thickness
Minimum GCL + IPL Thickness
B
GCC
GCC Thickness (µm)
120
90
60
30
0
***
***
***
Abnl
Ctrl
Abnl
Ctrl
Anterior
Posterior
C
Normalized GCC
Normalized GCC (µm/mo)
20
10
0
-10
-20
***
Anterior
Posterior
D
Nasal, Crossed GCC
GCC Thickness (µm)
120
90
60
30
***
***
***
Abnl
Ctrl
Abnl
Ctrl
Anterior
Posterior
E
Temporal, Non-Crossed GCC
GCC Thickness (µm)
120
90
60
30
0
***
***
***
Abnl
Ctrl
Abnl
Ctrl
Anterior
Posterior
F
Normalized GCC
Normalized GCC (µm/mo)
5
0
-5
-10
-15
***
***
Ant
Post
Ant
Post
Crossed
Non-Crossed

Figure 2

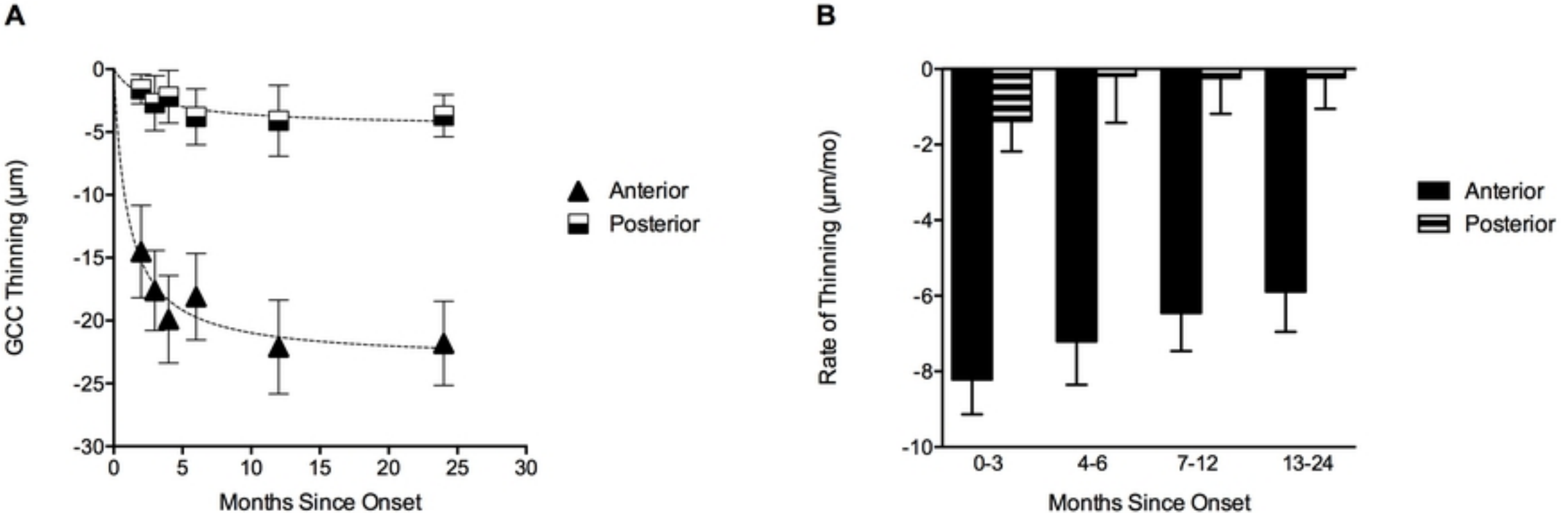
A
GCC Thinning (µm)
0
-5
-10
-15
-20
-25
-30
0
5
10
15
20
25
30
Months Since Onset
Anterior
Posterior
B
Rate of Thinning (µm/mo)
0
-2
-4
-6
-8
-10
0-3
4-6
7-12
13-24
Months Since Onset
Anterior
Posterior

Figure 3

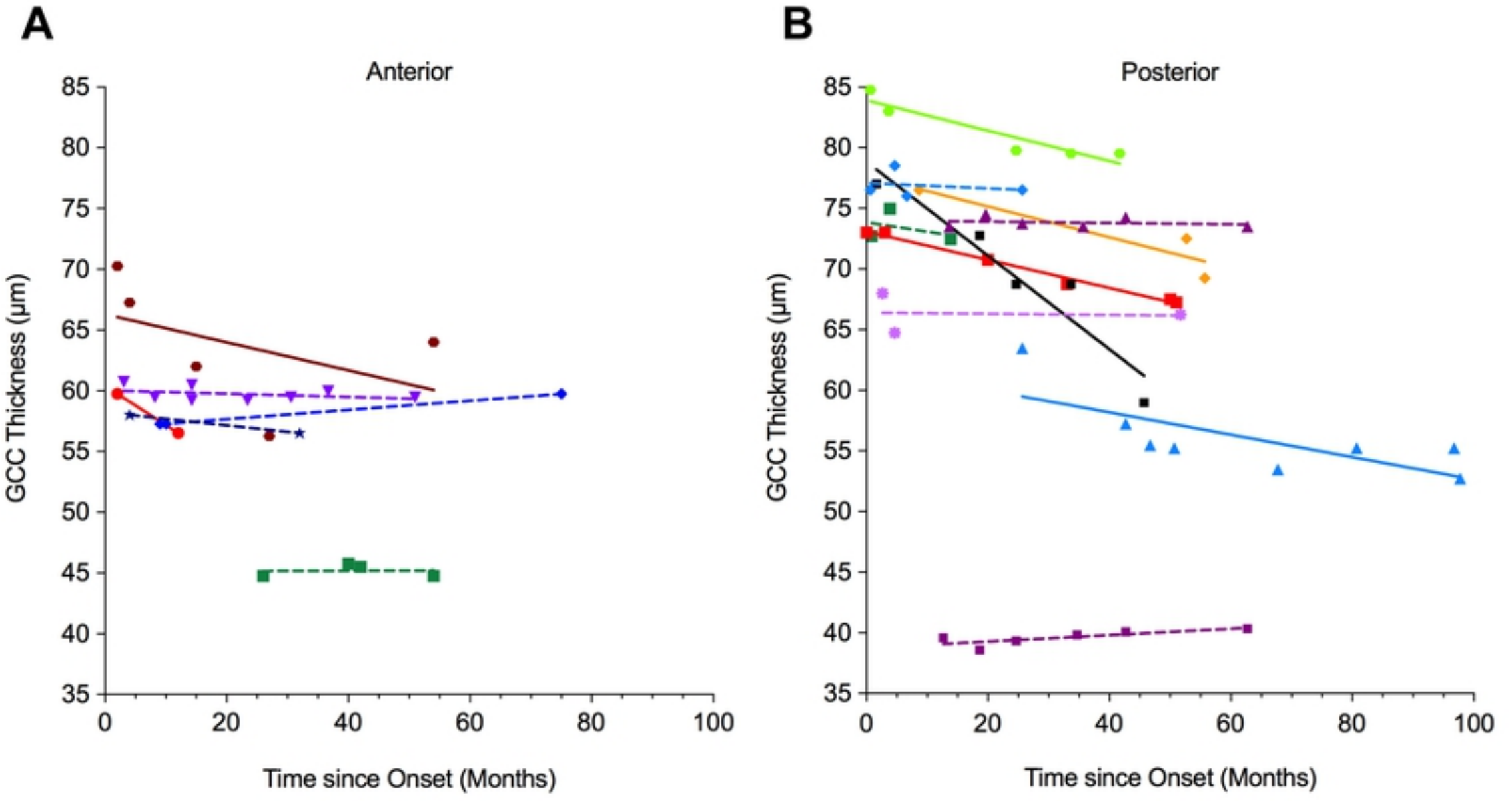
A
Anterior
GCC Thickness (µm)
Time since Onset (Months)
B
Posterior
GCC Thickness (µm)
Time since Onset (Months)

Figure 4

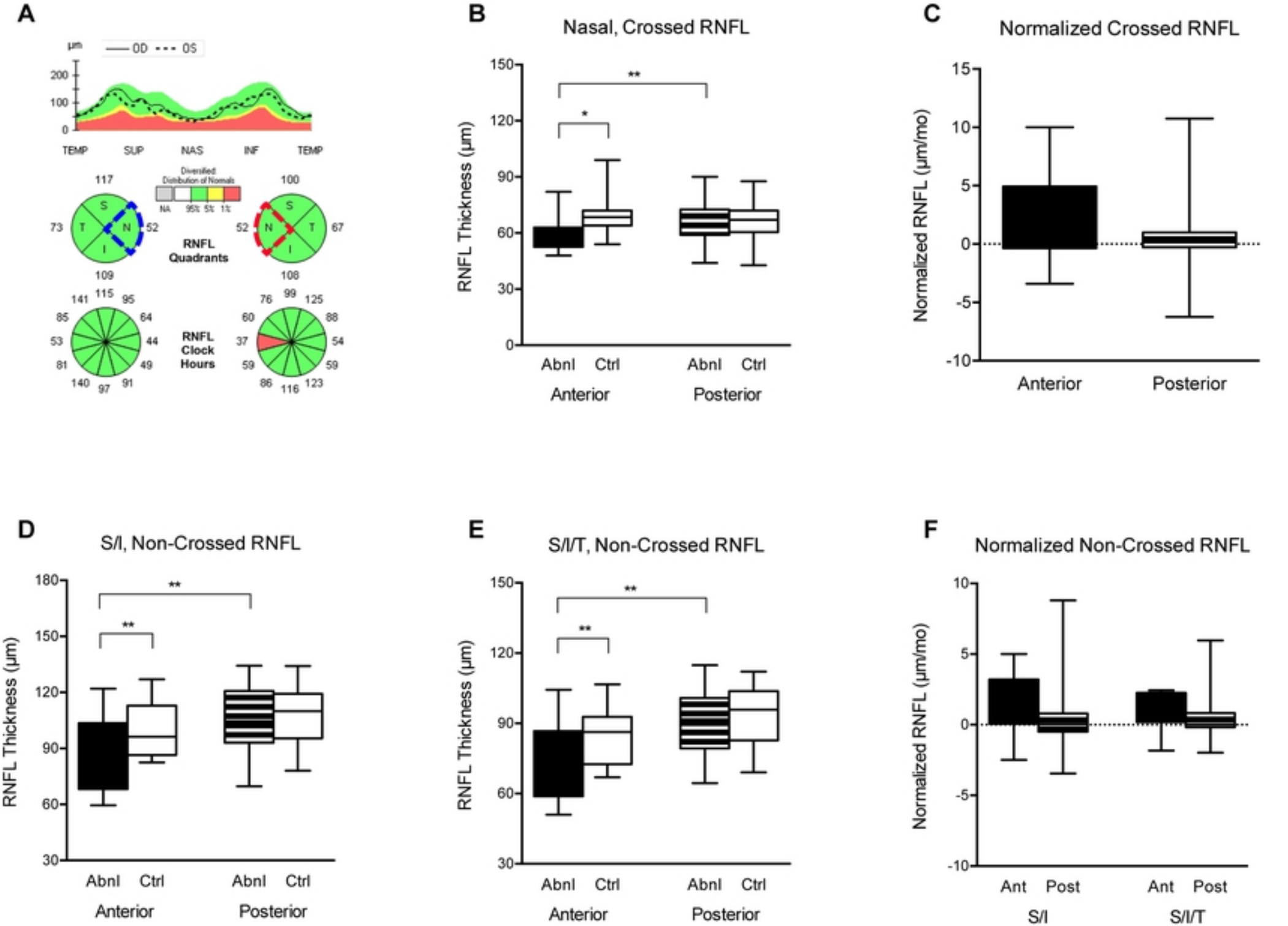
A
μm
OD
OS
200
100
0
TEMP
SUP
NAS
INF
TEMP
Diversified Distribution of Normals
NA
95%
5%
1%
117
73
52
109
100
52
67
108
S
T
N
I
RNFL Quadrants
141
115
95
85
64
53
44
81
49
140
97
91
RNFL Clock Hours
76
99
125
60
88
37
54
59
59
86
116
123
B
Nasal, Crossed RNFL
RNFL Thickness (μm)
150
120
90
60
30
0
**
*
Abnl
Ctrl
Abnl
Ctrl
Anterior
Posterior
C
Normalized Crossed RNFL
Normalized RNFL (μm/mo)
15
10
5
0
-5
-10
Anterior
Posterior
D
S/I, Non-Crossed RNFL
RNFL Thickness (μm)
180
150
120
90
60
30
**
**
Abnl
Ctrl
Abnl
Ctrl
Anterior
Posterior
E
S/I/T, Non-Crossed RNFL
RNFL Thickness (μm)
150
120
90
60
30
**
**
Abnl
Ctrl
Abnl
Ctrl
Anterior
Posterior
F
Normalized Non-Crossed RNFL
Normalized RNFL (μm/mo)
10
5
0
-5
-10
Ant
Post
Ant
Post
S/I
S/I/T

Figure 5